Characterization of atmospheric aerosol optical properties based on the combined use of a ground-based Raman lidar and an airborne optical particle counter in the framework of the Hydrological Cycle in the Mediterranean Experiment – Special Observation Period 1

Dario Stelitano[1,2], Paolo Di Girolamo[1], Andrea Scoccione[3], Donato Summa[2], Marco Cacciani[3]

[1] Scuola di Ingegneria, Università degli Studi della Basilicata, 85100 Potenza – Italy
[2] now at Osservatorio Nazionale Terremoti, Istituto Nazionale di Geofisica e Vulcanologia, 00143 Roma – Italy
[3] Dipartimento di Fisica, Università di Roma "La Sapienza", Piazzale Aldo Moro, n. 2, 00100 Roma – Italy

Correspondence to: Paolo Di Girolamo (paolo.digirolamo@unibas.it)

Abstract. Vertical profiles of particle backscattering coefficient at 355, 532 and 1064 nm measured by the lidar Raman system BASIL have been compared with simulated particle backscatter profiles obtained through a Mie scattering code based on the use of simultaneous and almost co-located profiles provided by an air-borne optical particle counter. . Measurements were carried out during dedicated flights of the French research aircraft ATR42 in the frame of the European Facility for Airborne Research (EUFAR) Project "WaLiTemp", as part of the Hydrological Cycle in the Mediterranean Experiment - Special Observation Period 1 (HyMeX-SOP1). Results from two selected case studies are reported and discussed in the paper and two slightly different analysis approaches are illustrated and applied to the dataset. Results reveal a good agreement between measured and simulated multi-wavelength particle backscattering profiles. Specifically, simulated and measured particle backscattering profiles at 355 and 532 nm are found to deviate less than 15 % (mean value=7 %) and 50 % (mean value=30%), respectively, when considering the presence of a Continental/Urban aerosol component. The reported good agreement between measured and simulated multi-wavelength particle backscatter profiles testifies the ability of multi-wavelength Raman lidar systems to infer aerosol types at different altitudes.

1 Introduction

Aerosols are a key atmospheric component, playing a major role in meteo-climatic processes. Aerosols influence precipitation processes and the water cycles primary through two effects: the direct effect, as a result of the scattering/absorption of solar radiation (among others, Haywood and Boucher, 2000; Takemura et al., 2005), and the indirect effect, as a result of the interaction with clouds (among others, Sekiguchi et al., 2003; Yang et al., 2011). A semi-direct effect can also arise in the presence of high aerosol loading, determining scattering and absorption enhancement, ultimately leading to an alteration of atmospheric stability (e.g. Mitchell, 1971). Despite the well-recognized aerosol importance in

meteorological processes and climate evolution, only a limited number of remote sensing techniques can provide vertically resolved measurements of the microphysical properties of aerosol particles (among others, Bellantone *et al*., 2008; Granados-Muñoz *et al*., 2016; Mhawish *et al*., 2018). For example, in-situ sensors transported by aerostatic balloons or any other flying vector allow measuring the vertical profile of aerosol size and microphysical properties, with high vertical resolution (of the order of 10 m), but typically with a limited temporal resolution. Any experiment aimed at characterizing the temporal evolution of aerosol microphysical properties would require several consecutive balloon launches or flights, with the time lag between two consecutive launches/flights unlikely being shorter than 1 hour, with a consequent detriment of the temporal resolution. Additionally, in-situ particle sensors are quite heavy and bulky, which - in the case of balloon-borne experiments - implies the use of quite large aerostatic balloons. This makes monitoring by in-situ particle sensors very expensive and logistically difficult to implement.

Remote sensing techniques can overcome these limitations. A variety of passive optical remote sensors (i.e. spectro-radiometers, sun and sky photometers, etc.) have demonstrated their capability to characterize aerosol microphysical properties, but they lack in vertical resolution, which makes them scarcely suited for vertically resolved measurements of aerosol size and microphysical properties. Low vertical resolution is combined with a limited temporal resolution when these techniques are implemented on sun-synchronous orbiting platforms, with a typical "revisit time" of several hours. Active remote sensing systems may overcome this limitation. Specifically, lidar systems with aerosol measurement capability are characterized by high accuracies and temporal/vertical resolutions, which makes them particularly suited for aerosol typing applications. Lidar measurements of aerosol optical properties have been reported since the early sixties (among others, Fiocco and Grams, 1964; Elterman, 1966). Originally, measurements were carried out with single-wavelength elastic backscatter lidars capable to provide vertical profiles of the particle backscattering coefficient at the laser wavelength. In these systems the particle backscattering coefficient is determined from the elastic lidar signals based on the application of the Klett-Fernald-Sasano approach (Klett, 1981, 1985; Fernald, 1984) or similar derived approaches (Di Girolamo *et al*., 1995, 1999). More recently, the acquired capability to measure roto-vibrational Raman lidar echoes from nitrogen and oxygen molecules made the determination of the particle extinction coefficient also possible (Ansmann, 1990; 1992). The possibility to retrieve particle size and microphysical parameters from multi-wavelength lidar data of particle backscattering, extinction and depolarization has been recently demonstrated by a variety of authors (Müller et al., 2001, 2007, 2009; Veselovskii et al., 2002, 2009, 2010). These measurements can be combined with simultaneous measurements of the atmospheric thermodynamic profiles (Wulfmeyer et al., 2005; Di Girolamo et al., 2008, 2018a) to characterize aerosol-cloud interaction mechanisms. The ground-based University of Basilicata Raman Lidar system (BASIL) has a demonstrated capability to provide multi-wavelength Raman lidar measurements with high-quality and accuracy for the retrieval of particle size and microphysical parameters (Veselovskii et al., 2010; Di Girolamo et al., 2012). The system was deployed in Candillargues (Southern France) in the period from August to November 2012 in the frame of the Hydrological cycle in the Mediterranean Experiment (HyMeX) Special Observation Period 1 (SOP1). In the present manuscript, measurements carried out by BASIL are illustrated with the purpose to characterize atmospheric aerosol optical properties. These measurements, in

combination with in-situ measurements from an airborne optical particle counter and the application of a Mie scattering code, are used to infer aerosol types. Back-trajectory analyses from a Lagrangian model ((HYSPLIT)) are used in support of the assessment of aerosol types (Man and Shih, 2001; Methven et al., 2001; Estellés et al., 2007; Toledano et al., 2009). The outline of the paper is the following: section 2 provides a description of the Raman lidar system BASIL and the airborne optical particle counter; section 3 illustrates HyMeX-SOP1. The methodology is illustrated in section 4, while measurements and simulations are reported in section 5. Finally, section 6 summarizes all results and provides some indications for possible future carry-on activities.

2 Instrumental setup

2.1 BASIL

The Raman lidar BASIL has been developed around a pulsed Nd:YAG laser, emitting pulses at 355, 532 and 1064 nm, with a repetition rate of 20 Hz. The system includes a large aperture telescope in Newtonian configuration, with a 400 mm diameter primary mirror, primarily aimed for the collection of Raman and higher range signals. Two additional smaller telescopes, developed around two 50 mm-diameter 200 mm-focal length lenses, are used to collect the backscatter echoes at 1064 nm and the total and cross-polarized backscatter echoes at 532 nm. The laser emission at 355 nm (average power of 10 W) is used to stimulate Raman scattering from water vapour, nitrogen and oxygen molecules (Di Girolamo et al., 2004, 2006, 2009a), which are ultimately used to measure the vertical profiles of atmospheric temperature, water vapour mixing ratio and aerosol extinction coefficient at 355 nm. Elastic backscattering echoes from aerosol and molecular species at 355, 532 and 1064 nm, in combination with the Raman scattering echoes from molecular nitrogen, are used to measure the vertical profiles of the aerosol backscattering coefficient at these three wavelengths. More details of the considered approaches are given in section 4. Raman echoes are very weak and degraded by solar radiation in daytime. Consequently, high laser powers and large aperture telescopes are required to measure daytime Raman signals with a sufficient signal-to-noise ratio throughout a large portion of the troposphere. The instrumental setup of BASIL has been described in detail in several previous papers (Di Girolamo et al., 2009a, 2009b, 2012a, 2012b; 2016; 2017; Bhawar et al., 2011).

2.2 Optical Particles Counter

An optical particle counter (OPC), manufactured by GRIMM Aerosol Technik GmbH (model Sky-OPC 1.129), is used to measure the size resolved particle number concentration dN/dr in the size range 0.25 - 32 μm. The sensor includes 31size bins. The laser beam generated by a 683 nm diode laser invests the aerosol particles exiting from a pump chamber; the scattered radiation is deflected by two separate mirrors and detected by a photon sensor (Heim et al., 2008). By summing up the particle number over all the size intervals, the total number concentration is derived (Grimm and Eatough, 2009). The OPC model used in the present effort has a specific airborne design (McMeeking et al., 2010). The use of a differential pressure sensor and an external pump allows OPC measurements to be performed independently of environmental pressure

conditions. The OPC was installed on-board the French research aircraft ATR42, operated by the Service des Avions Instrumentés pour la Recherche en Environnement (SAFIRE), as part of an ensemble of in-situ sensors for the characterization of aerosol and cloud size and microphysical properties. Dedicated flights by the ATR42 were performed during HyMeX-SOP 1 in the frame of the Wa-Li-Temp EUFAR project, with the aircraft looping up and down in the proximity of the Raman lidar system.

3 HyMeX and the Special Observation Period 1

The Hydrological cycle in Mediterranean Experiment was conceived with the overarching goal of collecting a large set of atmospheric and oceanic data to be used to get a better understanding of the hydrological cycle in the Mediterranean area. Within this experiment a major field campaign, the Special Observation Period 1 (SOP1), took place over the northwestern Mediterranean area in the period September–November 2012. During HyMeX-SOP1 the Raman lidar system BASIL was deployed in the Cévennes-Vivarais atmospheric 'supersite', located in Candillargues ($43^0$37' N, $4^0$04' E, elevation: 1m). BASIL was operated from 5 September to 5 November 2012, collecting more than 600 h of measurements, distributed over 51 measurement days and 19 Intensive Observation Periods (IOPs).

The French research aircraft ATR42, hosting the OPC, was stationed at Montpellier airport. Its main payload consisted of the airborne DIAL LEANDRE 2, profiling water vapour mixing ratio beneath the aircraft. The ATR42 payload also included in-situ sensors for turbulence measurements, as well as aerosol/cloud microphysics probes. Among these, the OPC. During HyMeX-SOP1, the ATR42 performed more than 60 flight hours: 8 were supported by the EUFAR project "WaLiTemp" and the remaining were supported by the "Mediterranean Integrated STudies at Regional and Local Scales" (MISTRALS) Program. A specific flight pattern was defined for the purposes of the "WaLiTemp" project (figure 1), with the aircraft making spirals (hippodromes) up and down around a central location, originally aimed to be the atmospheric supersite in Candillargues. Unfortunately, because of air-traffic restrictions, aircraft sensors' operation was typically started 20 km eastward of the supersite. Flights hours in the frame of the "WALiTemp" project were carried out on 13 September, 02 and 29 October and 05 November 2012.

Spiral ascents and descents were carried out with a vertical speed of 150 m/min. During each flight, except in presence of specific logistic issues, a minimum of two ascent-descent spirals were carried out. For the purposes of the present comparisons, in order to minimize effect associated with the sounding of different air masses, we selected days characterized by horizontally homogeneous atmospheric conditions.

4 Methodology

The particle volume backscattering coefficient can be expressed as:

$$\beta_{\lambda_0}^{par} = \int_0^{\infty} Q_{back}(r)\, n(r)\, \mathrm{d}r \tag{1}$$

with $Q_{back}(r)$ being the particle backscattering efficiency and $n'(r)=dN/dr$ being the particle size distribution. $Q_{back}(r)$ can be expressed as (Grainger *et al.*, 2004):

$$Q_{back} = \frac{2}{x^2} \sum_{n=1}^{\infty} (2n+1)\left(|a_n|^2 + |b_n|^2\right) \tag{2}$$

where the terms a_n and b_n represent the Mie scattering amplitudes of nth magnetic partial wave (n being the function order). a_n and b_n are obtained through the expressions:

$$a_n = \frac{\psi_n(x)\psi_n'(mx) - m\,\psi_n'(x)\psi_n(mx)}{\xi_n^{(1)}(x)\psi_n'(mx) - m\,\xi_n^{(1)\prime}(x)\psi_n(mx)} \tag{3}$$

$$b_n = \frac{\psi_n'(x)\psi_n(mx) - m\,\psi_n(x)\psi_n'(mx)}{\xi_n^{(1)\prime}(x)\psi_n'(mx) - m\,\xi_n^{(1)}(x)\psi_n(mx)} \tag{4}$$

where m is the complex refractive index; $x=2\,\pi\, r/\lambda$ is the particle size parameter, with λ being the laser wavelength and r being the particle radius, assumed to be a sphere. $\psi_n(x)$ and $\xi_n^{(1)}$ are Riccati–Bessel functions defined in terms of the spherical Bessel function of the first kind (Temme, 1996). A log-normal size distribution is considered in this study, with an analytical expression for each mode of the form (Grainger *et al.*, 2004):

$$n'(r) = \frac{N_0}{\sqrt{2\pi}} \frac{1}{\ln S} \frac{1}{r} \exp\left[-\frac{\left(\left[\ln r - \ln r_m\right]^2\right)}{2\ln^2 S} \right] \tag{5}$$

where $n'(r)=dN/dr$ is the number of particles within the size interval dr, with $N(r)$ representing the cumulative particle numberdistribution for particles larger than R, r_m is the median radius of the distribution, S is the standard deviation of the distribution and N_0 is the particle integral concentration for the considered mode. S is a measure of the particle polydispersity, with ln$S$ being equal to 1 for monodisperse particles The log-normal distribution is completely described by N_0, r_m and S. Three modes are typically considered to describe the different aerosol components (d'Almeida et al., 1991): a fine or nucleation particles mode, a large or accumulation particles mode and a giant or coarse particles mode.

For the purposes of this research effort, particle concentration N_0 is obtained by minimizing differences between the size distribution measured by the OPC and the simulated distribution, while the values of r_m and S are those identified in the following section based on literature results. Simulated backscatter profiles $\beta_{\lambda_0}^{par}(z)$ are the obtained through the application expression (1) for all altitudes covered by the OPC, considering different refractive index and size parameters' values for the three distribution modes, in dependence of the aerosol type, and integrating the expression over the three distribution modes. To perform these computations a specific Mie scattering code was developed by the authors in IDL environment. The possibility to retrieve the particle size and microphysical properties from multi-wavelength measurements of the particle backscattering and extinction coefficient has been demonstrated by several authors (among others, Müller et al., 2001, and

Veselovskii et al., 2002) based on the application of a retrieval scheme employing Tikhonov's inversion with regularization, which apply Mie scattering theory to ensemble of particles with spherical shape. However, an appropriate and effective application of this approach imposes the use of particle backscatter and extinction profiles with a statistical uncertainty not exceeding 5-10 %. Multi-wavelength Raman lidar measurements of the particle backscattering and extinction coefficient for the considered case studies were not characterized by such low level of uncertainty, this being especially true for the particle backscatter measurements at 1064 nm.

In order to determine aerosol typology, deviations between measured and simulated particle backscattering profiles at 355 nm and 532 nm were minimized. Initial values in terms of modal radius, $\bar{r}$, standard deviation, σ, and refractive index for the different aerosol components were taken from d'Almeida et al. (1991). At each altitude, the particle size distribution measured by the optical particle counter is compared with the five aerosol typologies listed in d'Almeida et al. (1991), which for the sake of clarity are reproduced below:

- Average continental (continental environment influenced by anthropic pollution),
- Urban (continental environment heavy influenced by anthropic pollution),
- Maritime-polluted (environment polluted as Mediterranean Sea or Northern Atlantic),
- Clean-polar (Artic environment during summer period),
- Clean continental-rural (rural continental environment without pollution).

Specifically, both urban and continental aerosols include a soot and pollution fine mode component (as both aerosol types include the same aerosol components, they are treated in what follows as a single aerosol type), a water soluble accumulation mode component and dust-like coarse mode component; the maritime polluted aerosol type includes a soot and pollution fine mode component, a water soluble accumulation mode component and a sea-salt coarse mode component; the summer-time Artic aerosol type includes a sulphate fine mode component and a sea salt and mineral accumulation mode component; the rural aerosol type includes a water soluble accumulation mode component and a dust-like coarse mode component.

d'Almeida et al. (1991), Junge and Jaenicke (1971) and Junge (1972) suggested the use of a tri-modal log-normal size distribution (see expression 5), indicating specific values for the two primary size distribution parameters, i.e. the modal radius, $\bar{r}$, and standard deviation, σ . Values of the modal radius, the standard deviation and the real, n_r, and imaginary part, n_i, of refractive index at the three lidar wavelengths (355, 532 and 1064 nm) for the three different aerosol components considered in the present computations are inferred from different literature papers (d'Almeida et al., 1991; Shettle and Fenn, 1976; Shettle and Fenn, 1979; WCP–112, 1986) and are listed in Table 1.

The log-normal size distribution has been computed considering the OPC data in the dimensional range 0.25 - 2.5 μm, with a 300 m vertical integration window. Results are illustrated in figure 2 (bold black line). In this same figure the size distribution computed from the OPC data is compared with the theoretical distributions for the three different modes (fine mode - red line, accumulation mode - violet line, coarse mode - light blue line).

For each of the three modes, the number of particles has been varied in order to have the total theoretical distribution (thin black line) matching the experimental distribution computed with the OPC data. The matching between the experimental and

185 theoretical distributions has been optimized based on the application of a best fit procedure. This approach was applied to each altitude level. In figure 2, we are considering experimental and theoretical distributions at an altitude of 1529 m, this being the lowest altitude where aerosols larger than 0.7 – 0.8 μm were measured by the OPC.

The vertical profiles of the particle backscattering coefficient at 355, 532 and 1064 nm have been simulated through the above mentioned Mie scattering code from the OPC data, considering values of $\bar{r}$ and σ for the different aerosol
190 components. Measured profiles of the particle backscattering coefficient profiles at 355 and 532 nm are obtained from the Raman lidar signals through the application of the Raman techniques, which relies on the ratio between the 355/532 nm elastic signal and the simultaneous molecular nitrogen roto-vibrational Raman signal. The two signals are characterized by an almost identical overlap function, and therefore the overlap effect cancel out when ratioing the signals. Conversely, particle backscattering coefficient profiles at 1064 nm are obtained through the application of a Klett-modified inversion
195 approach (Di Girolamo *et al*., 1995, 1999). The specific approach used in the present analysis considers a height-dependent lidar ratio profile and iterative procedure converging to a final particle backscattering profile Di Girolamo et al. (1995, 1995). It is to be specified that potential effects on our measurements associated with the incomplete overlap of the laser beam and field of view are negligible. In fact, the particle backscattering coefficient at both 355 and 532 nm are obtained through the Raman lidar technique, which considers the ratio of the elastic echoes over the corresponding N_2 Raman lidar
200 echoes, with the overlap function for the elastic channel and the corresponding N_2 Raman channel being substantially identical. Additionally, the elastic backscatter signal at 1064 nm and an additional elastic backscatter signal at 532 nm are collected with two small telescopes, developed around two 50 mm-diameter 200 mm-focal length lenses, with overlap regions not extending above 3-400 m.

A modified version of the approach defined by Di Iorio et al. (2003) was applied in order to determine the sounded aerosol
205 typology. This approach is based on the minimization of the relative deviation between the measured and the simulated particle backscattering coefficient, i.e.:

$$\Delta = \frac{1}{N_p}\sum_{k=1}^{N_p}\frac{|\beta_{\lambda(simulated)}(z_k) - \beta_{k(measured)}(z_k)|}{\beta_{\lambda(measured)}(z_k)}, \quad (6)$$

where z_k is the altitude.

In the attempt to simultaneously minimize deviations between measured and simulated particle backscattering profiles at
210 355, 532 and 1064 nm, a total deviation can be computed as the root sum square of the single deviations at the two wavelengths, which can be expressed as:

$$\Delta_{tot} = \sqrt{\Delta_{355}^2 + \Delta_{532}^2 + \Delta_{1064}^2}, \quad (7)$$

5 Results

5.1 Case Study on 13 September 2012

During the first ascending spiral, in-situ sensors on board the ATR42 were operated in the altitude region from 650 m to 5700 m above sea level (hereafter in the paper all altitudes are intended above sea level), covering the 40 min-time interval between 19.55 and 20.35 UTC. BASIL was operated in the time interval 19.00-23.00 UTC. Figure 3 illustrates the temporal evolution of the particle backscattering coefficient at 532 nm over the time interval 19.30-21.30 UTC. The figure is illustrated as a succession of 5 min vertical profiles with a vertical resolution of 7,5 m. The figure reveals the presence of a shallow nocturnal boundary layer, which is testified by the presence of an aerosol layer extending up to 500-600 m, and the presence of a residual layer extending up to 1500-2100 m.

Wind direction measurements performed by the on-board flight sensors reveal a primarily Northerly wind, with direction varying in the range ±30° depending on altitude. The NOAA HYSPLIT Lagrangian back-trajectory model (Draxler e Rolph, 1998; Rolph et al., 2017; Stein et al., 2015) has been used to determine the origin of the sounded air-masses. The HYSPLIT model computes air parcel trajectories, but can also be used to simulate complex transport, dispersion, chemical transformation and deposition mechanisms. A common application of the HYSPLIT model is the back- and forward-trajectory analysis, which is used to determine the origin or destination of the investigated air masses and establish source-receptor relationships.

In the present effort the HYSPLIT model is used to determine air masses trajectories at specific altitude levels in the days preceding their arrival on the lidar site in Candillargues. Specifically, figure 4 illustrates back-trajectories computed with the NOAA HYSPLIT model of the air masses overpassing the lidar site at 20 UTC on 13 September 2012 at an altitude of 600 m (red line), 4000 m (blue line) and 6000 m (green line). The trajectories extend back in time for 5 days, thus illustrating the air masses path since 20 UTC on 8 September 2012.

Air masses reaching the measurement site at altitudes of 600 and 4000 m originated in the vicinity of Iceland and Greenland and passed at low altitudes (< 400 m) over the North Atlantic Sea and over industrialized areas in France, while air masses at 5826 m originated in the North Atlantic Sea in the proximity of the Canadian coasts and persisted in marine environment for almost 5 days before reaching France.

Figure 5 compares the vertical profiles of the measured and simulated particle backscattering coefficient at 355 nm. The measured profile is obtained from the Raman lidar data integrated over the 40 min time interval coincident with the airplane ascent time (19.55-20.35 UTC on 13 September 2012), with a vertical resolution of 300 m. Simulated particle backscatter profiles include all five aerosol components specified above, i.e. the Continental/Urban components (red dashed line), the Continental (rural) component (green dashed line), the Arctic Summer component (black dashed line) and the Marine (polluted) component (blue dashed line). Figure 5 reveals a good agreement between the measured backscattering coefficient profile at 355 nm and those simulated at this same wavelength assuming a Continental/Urban aerosol component and a Marine (polluted) aerosol component.

This same analysis approach was also applied to the data at 532 nm. Figure 6 compares the vertical profiles of the measured (black line) and simulated (red line) particle backscattering coefficient at 532 nm over the same 40 min time interval on 13 September 2012, again with a vertical resolution of 300 m. Simulated particle backscatter profiles include the five above specified aerosol components. Lidar data at 532 nm are affected by a larger statistical uncertainty than those at 355 nm. Also in this case, the agreement between measured and simulated profiles appears quite good up to 3500-4000 m.

Figure 6 reveals that the measured particle backscattering coefficient profile at 532 nm is well reproduced by the simulated profiles at this same wavelength, especially those obtained considering a Continental/Urban aerosol component and a Marine (polluted) aerosol component, with simulated profiles slightly overestimate the measured profile, but being within or slightly exceeding the measurement error bar. Deviations between measured and simulated profiles are larger within the aerosol layer centred at 2800 m.

Figure 7 compares the vertical profiles of the measured and simulated particle backscattering coefficient at 1064 nm over the same 40 min time interval considered in figures 5 and 6, again with a vertical resolution of 300 m. Particle backscatter measurements at 1064 nm are affected by a statistical uncertainty larger than the one affecting the measurements at 532 nm. This large uncertainty is the result of the use of a reduced laser emission power at 1064 nm because of the restrictions imposed by the air traffic control authorities. In this case, the agreement between measured and simulated profiles is poorer, but still acceptable up to 2500 m.

Figure 8 illustrates the deviations between the measured and the simulated particle backscattering coefficient profile at 355 nm. The smallest deviations between the two profiles up to 4500 m are obtained when considering the presence of a Marine polluted aerosol component (smaller than 53 %, with a mean deviation of 23.2 %). Simulated profiles obtained considering a Continental/Urban aerosol component (not exceeding 54 %, with a mean deviation of 24.9 %) deviate less only within the altitude interval 1200-1300 m, while deviations are very similar above 2600 m. The simulated profile obtained considering the presence of either a Continental rural or an Arctic Summer aerosol component largely deviates from the measured profile (up to 80 % and 92%, respectively, with a mean deviation of 50.9% and 25.9%). The Artic component deviates less only above 4500 m, where the high signal noise level and the limited particle loading make aerosol type discrimination difficult to accomplish.

Figure 9 illustrates the deviations between the measured and the simulated particle backscattering coefficient profile at 532 nm. Again, the maximum altitude for aerosol type retrieval is 4340 m. The smallest deviations between measured and simulated particle backscattering coefficient profile are obtained when considering the presence of a Continental/Urban aerosol component (not exceeding 105 %, with a mean value of 30.8 %) or a Marine polluted aerosol component (smaller than 106 %, with a mean value of 30.9 %), while simulated profiles obtained considering the presence of either a Continental rural or an Arctic Summer aerosol component largely deviate from the measured profile (up to 60.6 % and 87%, respectively, with a mean deviation of 39.6 % and 79.2 %). The only exception is given by the interval 2300-3000 m, where the simulated profile obtained considering a Rural aerosol component deviates less.

Figure 10 illustrates the deviations between the measured and the simulated particle backscattering coefficient profile at 1064 nm considering the altitude up to 2500m. The smallest deviations between the two profiles over the considered altitude range are obtained when considering the presence of a Continental/Urban aerosol component (not exceeding 61.4 %, with a mean deviation of 21.2 %). Deviations between measured and simulated profile obtained considering a Marine polluted aerosol component are slightly larger (smaller than 55 %, with a mean deviation of 28.6 %), while the simulated profile obtained considering the presence of either a Continental rural or an Arctic Summer aerosol component largely deviate from the measured profile (up to 58 % and 82.7%, with a mean deviation of 40.9% and 67.3%, respectively). Again, the only exception is found in the interval 1600-1900 m, where the simulated profile obtained considering the Marine polluted aerosol component deviate less.

The overall deviation was calculated for the five distinct aerosol components. Figure 11 illustrates the overall deviations between the measured and the simulated particle backscattering coefficient profiles at 355, 532 nm and 1064 nm for the different aerosol components. In order to facilitate the interpretation of results, the overall deviation between measured and simulated particle backscattering coefficient profile, for the different aerosol components, has been plotted together with the measured particle backscattering profiles at all wavelength (figure 12). In the lowest portion of atmosphere up to 1700 m, i.e. inside the Planetary Boundary Layer, the Continental/Urban aerosol component is predominant. The upper layer between 1700 and 2400 m is characterized by the presence of a maritime aerosol component in the lower part and again a Urban aerosol component in the upper part. Deviations were computed above 2500 m, because of the high statistical noise of the 1064 nm lidar signal. Additional layers are visible in altitude range 2400-3100 m and 3800-4500 m. Above 2400 m simulations based on t Urban and Maritime components show similar deviations from measurements, except in the central part of layer between 2600 and 2900 m and between 4300 and 4500 m, where Rural aerosols deviate less. HYSPLIT back-trajectory analysis confirms that the sounded air masses in the previous days overpasses industrialized areas in France, Belgium, England.

5.2 Case Study on 02 October 2012

A second flight took place on 2 October 2012. During the ascending path, in-situ sensors on board the ATR42 were operated in the altitude region from 680 m to 5700 m, covering the 44 min time interval between 19.43 and 20.27 UTC. BASIL was operated over the time interval time interval 16.00-24.00 UTC.

Wind direction measurements performed by the on-board flight sensors reveal a North-Westerly wind, with direction varying in the range 220-320° depending on altitude. Figure 13 shows the 5-days back-trajectories from the NOAA HYSPLIT model at 600 m, 4000 m and 6000 m (in red, blue and green, respectively), ending on the lidar site at 20.00 UTC on 2 October 2012.

Back-trajectory analysis results reveal that air masses reaching the measurement site at an altitude of 600 m were originated in Northern Atlantic Ocean, South of Iceland, and have passed at low altitudes (500-600 m) over highly anthropized continental areas (Ireland, England and Northern France). A different path characterizes air masses at 4000 m. These were

originated over the Northern Atlantic Sea, offshore the Canadian coast. and have overpassed an area North of Azores, the Northern coast of Spain before reaching the measurement site. Finally, air masses reaching the measurement site at 6000 m originated over the North Pacific Ocean, have overpassed Canada, the North Atlantic Ocean, the Northern coast of Spain and have finally reached the measurement site.

In the analysis of this second case study, we applied the same methodology considered for the first case study.(1991). As for the previous case study, given the microphysical parameters and aerosol typology for each of the three given modes, the number of particles has been varied in order to have the theoretical distribution matching the experimental distribution computed with the OPC data, with the matching between the experimental and theoretical distributions again obtained through a best fit procedure. The modal radius, standard deviation and refractive index reported by d'Almeida et al. (1991) for the different considered aerosol components are listed in Table 1.

Figure 14 illustrates the vertical profiles of measured (black line) and simulated particle backscattering coefficient at 355 nm over the 44 min time interval between 19.43 and 20.27 UTC on 02 October 2012. Simulated particle backscatter profiles include all five aerosol components specified above, i.e. the Continental/Urban components (red dashed line), the Continental (rural) component (green dashed line), the Arctic Summer component (black dashed line) and the Marine (polluted) component (blue dashed line). Figure 14 reveals a good agreement between the measured backscattering coefficient profile at 355 nm and those simulated at this same wavelength assuming a Continental/Urban aerosol component and a Marine (polluted) aerosol component.

We applied this same analysis approach also to the data at 532 nm, with figure 15 illustrating the vertical profiles of the measured and simulated particle backscattering coefficient at 532 nm over the same time interval considered in figure 14. Again, simulated particle backscatter profiles include the five above specified aerosol components. Figure 15 reveals that the measured particle backscattering coefficient profile at 532 nm is well reproduced by the simulated profiles at this same wavelength, especially those obtained considering a Continental/Urban aerosol component and a Marine (polluted) aerosol component, with simulated profiles slightly underestimating the measured profile, but being within or slightly exceeding the measurement error bar. Deviations between measured and simulated profiles are larger within the aerosol layers centred at 3000m and 4000 m. Due to the limited laser power at 1064 nm for this specific measurement session, measured profiles the particle backscattering coefficient at 1064 nm are characterized by high statistical noise, which prevents from considering the comparison between measured and simulated particle backscatter profiles at this wavelength to be sued in the presents analysis.

Figure 16 illustrates the deviations between the measured and the simulated particle backscattering coefficient profiles at 355 nm. The smallest deviations between the measured and the simulated particle backscattering coefficient profile over the considered altitude range are obtained when considering the presence of a Continental/Urban aerosol component (not exceeding 15 % up to 5000 m, with a mean deviation of 5.9 %). Deviations between the measured and simulated profile obtained considering a Marine polluted aerosol component are slightly exceeding these values (smaller than 20 % up to 5000 m, with a mean deviation of 9.5 %), while the simulated profile obtained considering the presence of either a Continental

rural or an Arctic Summer aerosol component largely deviates from the measured profile (up to 80 %, with a mean deviation of 50.9% and 25.9%, respectively).

Figure 17 illustrates the deviations between measured and simulated particle backscattering coefficient profile at 532 nm. Again, the smallest deviations between the two profiles over the considered altitude range are obtained when considering a Continental/Urban aerosol component (not exceeding 50 % up to 5000 m, with a mean deviation of 25.9 %), with the only exception for the interval 3100-3700 m, where the simulated profile obtained considering a Marine polluted aerosol component deviates less. Above 3700 m simulated profiles obtained considering a Continental/Urban and a Marine polluted aerosol component equally deviate from the measured profile.

In the attempt to simultaneously minimize deviations between measured and simulated particle backscattering profiles at both 355 and 532 nm, following expression 7, a total deviation can be computed as the root sum square of the single deviations at the two wavelengths, which can be expressed as:

$$\Delta_{tot} = \sqrt{\Delta_{355}^2 + \Delta_{532}^2}, \quad (8)$$

This quantity was calculated for the five distinct aerosol components. Figure 18 illustrates the total deviations between the measured and the simulated particle backscattering coefficient profiles at 355 and 532 nm for the different aerosol components. In order to facilitate the interpretation of these results, the total deviation between measured and simulated particle backscattering coefficient profiles for the different aerosol components has been plotted together with the measured particle backscattering profiles at both 355 and 532 nm (figure 19).

Figure 19 allows revealing the following considerations. In the lowest portion of the atmosphere, up to an altitude of ~1300 m (altitude 1), aerosol particles are most likely characterized by a predominant Continental/Urban component. This aerosol layer extends up to ~1600 m, which is the altitude where the boundary layer height is located as also indicated by the simultaneous radiosonde data (not shown here). In the upper portion of the boundary layer, in the vertical interval 1300-1600 m, deviations associated with Continental/Urban, Marine polluted and Continental rural component overlap, which suggests that all three aerosol components are possible. However, while this upper portion of the boundary layer is typically characterized by entrainment effects (interfacial region), which may allow different aerosol components to be ingested, the Continental/Urban component is likely to be the predominant component.

Above the top of the boundary layer and up to ~2700 m (altitude 2), particle backscatter decreases with altitude.. The typology analysis suggests Continental/Urban aerosols likely to be the predominant component, as in fact total deviation between the measured and the simulated particle backscattering coefficient profile for this aerosol component is far lower than for all other aerosol components.

In the altitude interval 2700-3600 m (altitudes 2-3, with max. at 3000 m) the measured particle backscatter profiles reveal the presence of a distinct aerosol layer. The typology analysis indicates both the Continental/Urban and the Marine polluted components to be possible. An additional distinct aerosol layer is found in the altitude interval 3600-4600 m (altitudes 3-4, with max. at 4000 m). Again, the typology analysis suggests the Continental/Urban component to be possible. Sounded

aerosol particles at 3000 and 4000 m are compatible with continental polluted aerosols, this possibility being confirmed by the back-trajectory analysis at 3000 and 4000 m.

A sensitivity study has been also carried out to assess the sensitivity of the results to changes of specific size and microphysical parameters' values. The sensitivity study reveals that the considered methodology for aerosol typing is successfully applicable in the altitude region up to 3900 m, as in fact above this altitude the statistical uncertainty affecting the lidar signals is high and this severely reduces the sensitively of the aerosol typing methodology. The sensitivity analysis also reveals that in the lower levels, typically within the boundary layer where aerosol loading is larger, deviations between measured and simulated particle backscattering coefficient at the three wavelengths may vary by up to 20 % as a result of a ± 5 % variability of specific size and microphysical parameters (for example, the real part of the refractive index), which certainly reduces confidence in the aerosol type assessment, but is not compromising its outcome. Based on the results from this study we may conclude that the use of particle backscattering measurements at two wavelengths in combination with OPC measurements allow to get a sufficiently reliable assessment of the aerosol types, which can be verified and refined based on the use of back-trajectory analyses.

6 Summary

During HyMeX-SOP1, the Raman lidar system BASIL was deployed in Candillargues (Southern France) and operated almost continuously over a two month period in the time frame October-November 2012. Dedicated flights of the French research aircraft ATR42 were carried out in the frame of the EUFAR-WaLiTemp Project. The ATR42 payload included *in situ* sensors for turbulence measurements, as well as aerosol/cloud microphysics probes. Among these, an optical particle counter (GRIMM Aerosol Technik GmbH, model: Sky-OPC 1.129) capable of measuring particle number concentration in the size interval 0.25 - 2.5 μm. A specific flight pattern was considered for the purpose of this study, with the aircraft making spirals up and down around a central location approximately 20 km eastward of the lidar site. Vertical profiles of the particle backscattering coefficient at 355, 532 and 1064 nm have been simulated through the use of a Mie scattering code, using the data provided by the optical particle counter. The simulated particle backscatter profiles have been compared with the profiles measured by the lidar Raman system BASIL. Results from two selected case studies (on 13 September and on 02 October 2012) were reported and discussed. An analysis approach based on the application of a Mie scattering code is considered and applied. The approach ultimately allows inferring the sounded aerosol types. The added value of the reported methodology is represented by the possibility to infer the presence of different aerosol types based on the use of multi-wavelength Raman lidar measurement from a ground-based system in combination with an independent measurement of the particle concentration profile (in our case we are using the one coming from an optical particle counter mounted onboard an aircraft overpassing the lidar site). This methodology is applicable when sounded particles are spherical or almost spherical, which allows for the Mie scattering theory to be applied for the determination of the particle backscattering coefficient.

The HYSPLIT-NOAA back-trajectory model was used to verify the origin of the sounded aerosol particles. Five different aerosol typologies are considered, i.e. Continental polluted, Clean continental-rural, Urban, Maritime-polluted and Clean-polar, with their size and microphysical properties taken from literature. The approach leads to an assessment of the predominant aerosol component based on the application of a minimization approach applied to the deviations between measured and the simulated particle backscattering profiles at 355 and 532 nm and for first test case study also at 1064 nm, considering all five aerosol typologies.

The application of this approach to the case study on 13 September 2012 suggests the presence of Urban and Maritime aerosols throughout the entire vertical extent of sounded column, except in the altitude region 2600-2900 m and 4300-4500 m ranges, where the presence of a Rural component is likely to be possible. The application of the approach to the case study on 02 October 2012 reveals that Continental/Urban aerosols are likely to be the predominant components up to ~1600 m, while the two distinct aerosol layers located in the altitude regions 2700-3600 m (with max. at 3000 m) and 3600-4600 m (with max. at 4000 m) are identified to likely consists of Continental/Urban and/or Marine polluted aerosols, respectively. The correctness of the results has been verified based on the application of the HYSPLIT-NOAA back-trajectory model, with the analysis extend backing in time for 5 days and allowing to assess the origin of the sounded aerosol particles.

Finally, a sensitivity study has been carried out to assess the sensitivity of the aerosol typing approach to varying size and microphysical parameters. The study reveals that the reported approach is successfully applicable in the altitude region up to ~ 4 km, while above this altitude the sensitively of the approach is sensitively reduced by the high statistical uncertainty affecting lidar signals. The sensitivity study also reveals that the within the boundary layer deviations between measured and simulated particle backscattering coefficient at 355, 532 and 1064 nm may vary up to 20 % as a result of a ± 5 % variability of specific size and microphysical parameters. Such results reveal that application of the reported approach, based on the use of particle backscattering measurements at two wavelengths in combination with OPC measurements, allow to get a sufficiently reliable assessment of aerosol typing.

Acknowledgement

This work is a contribution to the HyMeX Program supported by MISTRALS and ANR IODA-MED Grant ANR-11-BS56-0005. This research effort was supported by the European Commission under the European Facility for Airborne Research Program of the seventh Framework Program (Project WaLiTemp). This research effort was also supported by Project the "Smart Cities – Basilicata" from the Italian Ministry of Education, University and Research. The authors gratefully acknowledge NOAA Air Resources Laboratory (ARL) for the provision of the HYSPLIT transport and dispersion model used in this publication.

References

Ansmann, A., Riebesell, M. and Weitkamp, C.: Measurement of atmospheric aerosol extinction profiles with a Raman lidar, Opt. Lett., OL, 15(13), 746–748, doi:10.1364/OL.15.000746, 1990.

Ansmann, A., Wandinger, U., Riebesell, M., Weitkamp, C. and Michaelis, W.: Independent measurement of extinction and backscatter profiles in cirrus clouds by using a combined Raman elastic-backscatter lidar, Appl. Opt., AO, 31(33), 7113–7131, doi:10.1364/AO.31.007113, 1992.

Behrendt, A., Wulfmeyer, V., Bauer, H.-S., Schaberl, T., Di Girolamo, P., Summa, D., Kiemle, C., Ehret, G., Whiteman, D. N., Demoz, B. B., Browell, E. V., Ismail, S., Ferrare, R., Kooi, S. and Wang, J.: Intercomparison of Water Vapor Data Measured with Lidar during IHOP_2002. Part I: Airborne to Ground-Based Lidar Systems and Comparisons with Chilled-Mirror Hygrometer Radiosondes, J. Atmos. Oceanic Technol., 24(1), 3–21, doi:10.1175/JTECH1924.1, 2007.

Bellantone V, I. Carofalo, F. De Tomasi, M. R. Perrone, M. Santese, A. M. Tafuro, and A. Turnone, In situ samplings and remote sensing measurements to characterize aerosol properties over South-East Italy, Journal of Atmospheric and Oceanic Technology, 25, No.8, 1341-1356, 2008.

Bhawar, R., Di Girolamo, P., Summa, D., Flamant, C., Althausen, D., Behrendt, A., Kiemle, C., Bosser, P., Cacciani, M., Champollion, C., Di Iorio, T., Engelmann, R., Herold, C., Müller, D., Pal, S., Wirth, M. and Wulfmeyer, V.: The water vapour intercomparison effort in the framework of the Convective and Orographically-induced Precipitation Study: airborne-to-ground-based and airborne-to-airborne lidar systems, Quarterly Journal of the Royal Meteorological Society, 137(S1), 325–348, doi:10.1002/qj.697, 2011.

d'Almeida, G. A., Koepke, P. and Shettle E. P.: Atmospheric aerosols: Global climatology and radiative characteristics, A Deepak Publishing, Hampton, Virginia, 561 pp., 1991.

Di Girolamo, P., Gagliardi, R. V., Pappalardo, G., Spinelli, N., Velotta, R. and Berardi, V.: Two wavelength lidar analysis of stratospheric aerosol size distribution, Journal of Aerosol Science, 26(6), 989–1001, doi:10.1016/0021-8502(95)00025-8, 1995.

Di Girolamo, P., Ambrico, P. F., Amodeo, A., Boselli, A., Pappalardo, G. and Spinelli, N.: Aerosol observations by lidar in the nocturnal boundary layer, Appl. Opt., AO, 38(21), 4585–4595, doi:10.1364/AO.38.004585, 1999.

Di Girolamo, P., Marchese, R., Whiteman, D. N. and Demoz, B. B.: Rotational Raman Lidar measurements of atmospheric temperature in the UV, Geophysical Research Letters, 31(1), doi:10.1029/2003GL018342, 2004.

Di Girolamo, P., Behrendt, A. and Wulfmeyer, V.: Spaceborne profiling of atmospheric temperature and particle extinction with pure rotational Raman lidar and of relative humidity in combination with differential absorption lidar: performance simulations, Appl. Opt., AO, 45(11), 2474–2494, doi:10.1364/AO.45.002474, 2006.

Di Girolamo, P., Behrendt, A., Kiemle, C., Wulfmeyer, V., Bauer, H., Summa, D., Dörnbrack, A. and Ehret, G.: Simulation of satellite water vapour lidar measurements: Performance assessment under real atmospheric conditions, Remote Sensing of Environment, 112(4), 1552–1568, doi:10.1016/j.rse.2007.08.008, 2008.

Di Girolamo, P., Summa, D. and Ferretti, R.: Multiparameter Raman Lidar Measurements for the Characterization of a Dry Stratospheric Intrusion Event, J. Atmos. Oceanic Technol., 26(9), 1742–1762, doi:10.1175/2009JTECHA1253.1, 2009a.

Di Girolamo, P., Summa, D., Lin, R.-F., Maestri, T., Rizzi, R. and Masiello, G.: UV Raman lidar measurements of relative humidity for the characterization of cirrus cloud microphysical properties, Atmos. Chem. Phys., 9(22), 8799–8811, doi:10.5194/acp-9-8799-2009, 2009b.

Di Girolamo, P., Summa, D., Bhawar, R., Di Iorio, T., Cacciani, M., Veselovskii, I., Dubovik, O. and Kolgotin, A.: Raman lidar observations of a Saharan dust outbreak event: Characterization of the dust optical properties and determination of particle size and microphysical parameters, Atmospheric Environment, 50, 66–78, doi:10.1016/j.atmosenv.2011.12.061, 2012a.

Di Girolamo, P., Summa, D., Cacciani, M., Norton, E. G., Peters, G. and Dufournet, Y.: Lidar and radar measurements of the melting layer: observations of dark and bright band phenomena, Atmospheric Chemistry and Physics, 12(9), 4143–4157, doi:https://doi.org/10.5194/acp-12-4143-2012, 2012b.

Di Girolamo, P., Flamant, C., Cacciani, M., Richard, E., Ducrocq, V., Summa, D., Stelitano, D., Fourrié, N. and Saïd, F.: Observation of low-level wind reversals in the Gulf of Lion area and their impact on the water vapour variability, Quarterly Journal of the Royal Meteorological Society, 142(S1), 153–172, doi:10.1002/qj.2767, 2016.

Di Girolamo, P., Cacciani, M., Summa, D., Scoccione, A., De Rosa, B., Behrendt, A. and Wulfmeyer, V.: Characterisation of boundary layer turbulent processes by the Raman lidar BASIL in the frame of HD(CP)2 Observational Prototype Experiment, Atmospheric Chemistry and Physics, 17(1), 745–767, doi:https://doi.org/10.5194/acp-17-745-2017, 2017.

Di Girolamo, P., Behrendt, A. and Wulfmeyer, V.: Space-borne profiling of atmospheric thermodynamic variables with Raman lidar: performance simulations, Opt. Express, OE, 26(7), 8125–8161, doi:10.1364/OE.26.008125, 2018a.

Di Girolamo, P., Scoccione, A., Cacciani, M., Summa, D., De Rosa, B. and Schween, J. H.: Clear-air lidar dark band, Atmospheric Chemistry and Physics, 18(7), 4885–4896, doi:https://doi.org/10.5194/acp-18-4885-2018, 2018b.

Di Iorio, T., Di Sarra, A., Junkermann, W., Cacciani, M., Fiocco, G. and Fuà, D.: Tropospheric aerosols in the Mediterranean: 1. Microphysical and optical properties, Journal of Geophysical Research: Atmospheres, 108(D10), doi:10.1029/2002JD002815, 2003.

Draxler, R. R and Hess, G. D.: An overview of the HYSPLIT_4 modeling system for trajectories, dispersion and deposition. Australian meteorological magazine, 47(4), 295–308, 1998.

Elterman, L.: Aerosol Measurements in the Troposphere and Stratosphere, Appl. Opt., AO, 5(11), 1769–1776, doi:10.1364/AO.5.001769, 1966.

Estellés, V., J. A. Martı´nez-Lozano, and M. P. Utrillas, 2007: Influence of air mass history on the columnar aerosol properties at Valencia, Spain. J. Geophys. Res., 112, D15211, doi:10.1029/ 2007JD008593.

Fernald, F. G.: Analysis of atmospheric lidar observations: some comments, Appl. Opt., AO, 23(5), 652–653, doi:10.1364/AO.23.000652, 1984.

Fiocco, G. and Grams, G.: Observations of the Aerosol Layer at 20 km by Optical Radar, J. Atmos. Sci., 21(3), 323–324, doi:10.1175/1520-0469(1964)021<0323:OOTALA>2.0.CO;2, 1964.

Granados-Muñoz, M. J., Bravo-Aranda, J. A., Baumgardner, D., Guerrero-Rascado, J. L., Pérez-Ramírez, D., Navas-Guzmán, F., Veselovskii, I., Lyamani, H., Valenzuela, A., Olmo, F. J., Titos, G., Andrey, J., Chaikovsky, A., Dubovik, O., Gil-Ojeda, M., and Alados-Arboledas, L.: A comparative study of aerosol microphysical properties retrieved from ground-based remote sensing and aircraft in situ measurements during a Saharan dust event, Atmos. Meas. Tech., 9, 1113-1133, https://doi.org/10.5194/amt-9-1113-2016, 2016.

Grimm, H. and Eatough, D. J.: Aerosol Measurement: The Use of Optical Light Scattering for the Determination of Particulate Size Distribution, and Particulate Mass, Including the Semi-Volatile Fraction, Journal of the Air & Waste Management Association, 59(1), 101–107, doi:10.3155/1047-3289.59.1.101, 2009.

Haywood, J. and Boucher, O.: Estimates of the direct and indirect radiative forcing due to tropospheric aerosols: A review, Reviews of Geophysics, 38(4), 513–543, doi:10.1029/1999RG000078, 2000.

Heim, M., Mullins, B. J., Umhauer, H. and Kasper, G.: Performance evaluation of three optical particle counters with an efficient "multimodal" calibration method, Journal of Aerosol Science, 39(12), 1019–1031, doi:10.1016/j.jaerosci.2008.07.006, 2008.

Junge, C. and Jaenicke, R.: New results in background aerosols studies from the Atlantic expedition of the R.V. Meteor, Spring 1969, Journal of Aerosol Science, 2(3), 305–314, doi:10.1016/0021-8502(71)90055-3, 1971.

Junge, C. E.: Our knowledge of the physico-chemistry of aerosols in the undisturbed marine environment, Journal of Geophysical Research, 77(27), 5183–5200, doi:10.1029/JC077i027p05183, 2012.

Klett, J. D.: Stable analytical inversion solution for processing lidar returns, Appl. Opt., AO, 20(2), 211–220, doi:10.1364/AO.20.000211, 1981.

Klett, J. D.: Lidar inversion with variable backscatter/extinction ratios, Appl. Opt., AO, 24(11), 1638–1643, doi:10.1364/AO.24.001638, 1985.

Man, C.K., and Shih, M.Y.: Identification of sources of PM10 aerosols in Hong Kong by wind trajectory analysis, Journal of Aerosol Science, Volume 32, Issue 10, Pages 1213-1223, https://doi.org/10.1016/S0021-8502(01)00052-0, 2001.

McMeeking, G. R., Hamburger, T., Liu, D., Flynn, M., Morgan, W. T., Northway, M., Highwood, E. J., Krejci, R., Allan, J. D., Minikin, A. and Coe, H.: Black carbon measurements in the boundary layer over western and northern Europe, Atmos. Chem. Phys., 10(19), 9393–9414, doi:10.5194/acp-10-9393-2010, 2010.

Methven, J., Evans, M., Simmonds, P. and Spain, G. : Estimating relationships between air mass origin and chemical composition. J. Geophys. Res., 106, 5005–5019, 2001.

Mhawish, A., Kumar, M., Mishra A. K., Srivastava P. K. andBanerjee T.: Chapter 3 - Remote Sensing of Aerosols From Space: Retrieval of Properties and Applications, Remote Sensing of Aerosols, Clouds, and Precipitation, Elsevier, Pages 45-83, ISBN 9780128104378, https://doi.org/10.1016/B978-0-12-810437-8.00003-7, 2018.

Mitchell, J. M.: The Effect of Atmospheric Aerosols on Climate with Special Reference to Temperature near the Earth's Surface, J. Appl. Meteor., 10(4), 703–714, doi:10.1175/1520-0450(1971)010<0703:TEOAAO>2.0.CO;2, 1971.

Müller, D., Wandinger, U., Althausen, D. and Fiebig, M.: Comprehensive particle characterization from three-wavelength Raman-lidar observations: case study, Appl. Opt., AO, 40(27), 4863–4869, doi:10.1364/AO.40.004863, 2001.

Müller D., Mattis, I., Ansmann, A., Wandinger, U., Ritter, C. and Kaiser, D.: Multiwavelength Raman lidar observations of particle growth during long-range transport of forest-fire smoke in the free troposphere, Geophysical Research Letters, 34(5), doi:10.1029/2006GL027936, 2007.

Müller, T., Schladitz, A., Massling, A., Kaaden, N., Kandler, K. and Wiedensohler, A.: Spectral absorption coefficients and imaginary parts of refractive indices of Saharan dust during SAMUM-1, Tellus B: Chemical and Physical Meteorology, 61(1), 79–95, doi:10.1111/j.1600-0889.2008.00399.x, 2009.

Rolph, G., Stein, A., and Stunder, B.,: Real-time Environmental Applications and Display sYstem: READY. Environmental Modelling & Software, 95, 210-228, https://doi.org/10.1016/j.envsoft.2017.06.025 (http://www.sciencedirect.com/science/article/pii/S1364815217302360), 2017.

Sekiguchi, M., Nakajima, T., Suzuki, K., Kawamoto, K., Higurashi, A., Rosenfeld, D., Sano, I. and Mukai, S.: A study of the direct and indirect effects of aerosols using global satellite data sets of aerosol and cloud parameters, Journal of Geophysical Research: Atmospheres, 108(D22), doi:10.1029/2002JD003359, 2003.

Stein, A. F., Draxler, R. R., Rolph, G. D., Stunder, B. J. B., Cohen, M. D. and Ngan, F.: NOAA's HYSPLIT Atmospheric Transport and Dispersion Modeling System, Bull. Amer. Meteor. Soc., 96(12), 2059–2077, doi:10.1175/BAMS-D-14-00110.1, 2015.

Takemura, T., Nozawa, T., Emori, S., Nakajima, T.Y. and Nakajima, T.: Simulation of climate response to aerosol direct and indirect effects with aerosol transport-radiation model, Journal of Geophysical Research: Atmospheres, 110(D2), doi:10.1029/2004JD005029, 2005.

Temme, N. M., Special Functions: An introduction to the classical functions of mathematical physics (2nd print ed.). New York: Wiley. pp. 228–231. ISBN 0471113131, 1996.

Toledano, C., Cachorro, V. E., De Frutos, A. M., Torres, B. andBerjon, A., Sorribas, M., Stone, R. S., Airmass Classification and Analysis of Aerosol Types at El Arenosillo (Spain), Journal Of Applied Meteorology And Climatology, Volume 48, 962-981, doi: 10.1175/2008jamc2006.1, 2009.

Veselovskii, I., Kolgotin, A., Griaznov, V., Müller, D., Wandinger, U. and Whiteman, D. N.: Inversion with regularization for the retrieval of tropospheric aerosol parameters from multiwavelength lidar sounding, Appl. Opt., AO, 41(18), 3685–3699, doi:10.1364/AO.41.003685, 2002.

Veselovskii, I., Whiteman, D. N., Kolgotin, A., Andrews, E. and Korenskii, M.: Demonstration of Aerosol Property Profiling by Multiwavelength Lidar under Varying Relative Humidity Conditions, J. Atmos. Oceanic Technol., 26(8), 1543–1557, doi:10.1175/2009JTECHA1254.1, 2009.

Veselovskii, I., Dubovik, O., Kolgotin, A., Lapyonok, T., Di Girolamo, P., Summa, D., Whiteman, D. N., Mishchenko, M. and Tanré, D.: Application of randomly oriented spheroids for retrieval of dust particle parameters from multiwavelength lidar measurements, Journal of Geophysical Research: Atmospheres, 115(D21), doi:10.1029/2010JD014139, 2010.

WCP-112, A Preliminary Cloudless Standard Atmosphere for Radiation Computation. WCP/IAMAP Radiation Commission. Geneva: WCP, (ICSU /WMO/WCP/IAMAP) (WCP-112). ii, 53 p. Call no: WCP 112 TD 241986, 1986.

Wulfmeyer, V., Bauer, H., Di Girolamo, P. and Serio, C.: Comparison of active and passive water vapor remote sensing from space: An analysis based on the simulated performance of IASI and space borne differential absorption lidar, Remote Sensing of Environment, 95(2), 211–230, doi:10.1016/j.rse.2004.12.019, 2005.

Yang, F., Tan, J., Zhao, Q., Du, Z., He, K., Ma, Y., Duan, F., Chen, G. and Zhao, Q.: Characteristics of PM2.5 speciation in representative megacities and across China, Atmos. Chem. Phys., 11(11), 5207–5219, doi:10.5194/acp-11-5207-2011, 2011.

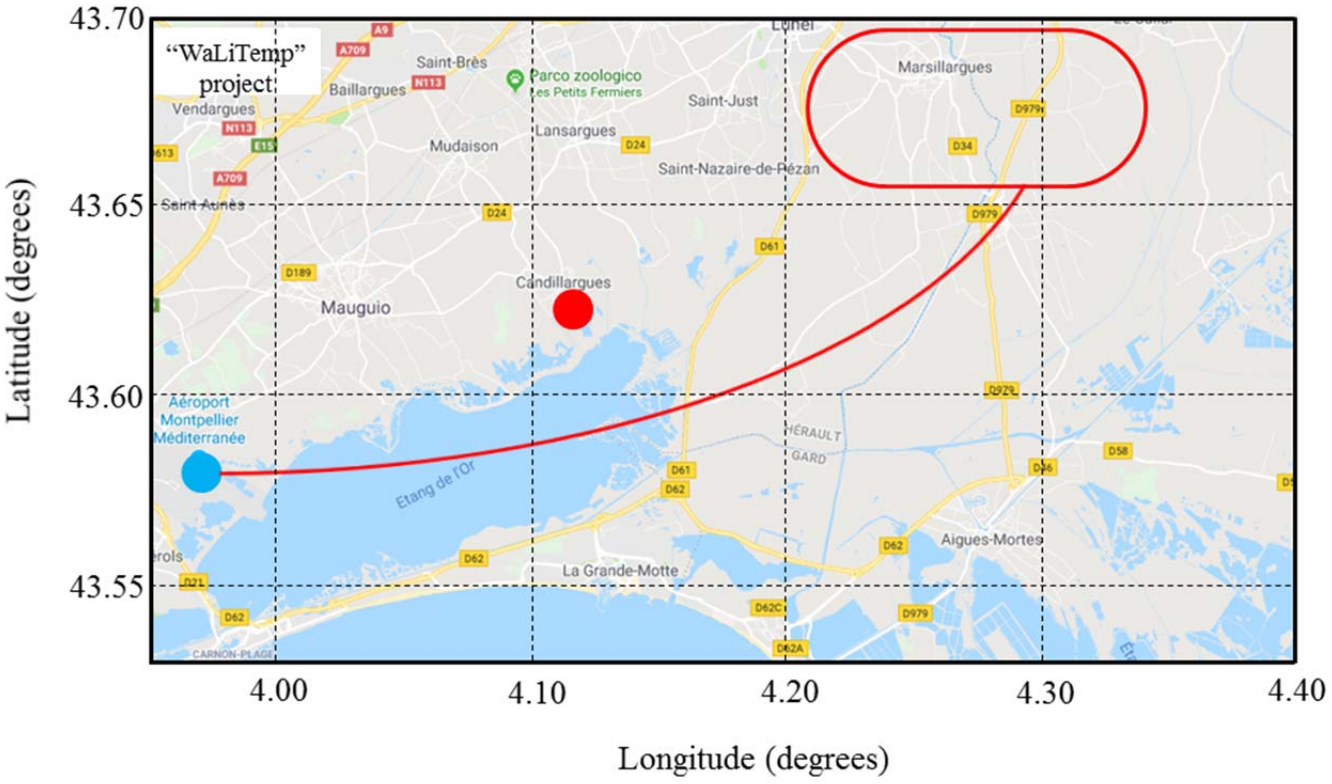

Figure 1: ATR42 flight pattern in the frame of the "WaLiTemp" project (red line). The light blue dot represents the position of Montpellier Airport, where the ATR-42 was taking-off and landing, while the red dot represent the position of the Raman lidar BASIL. The red curve represents the footprint of the aircraft pattern, including the positions of the spirals (hippodromes) up and down and the ground track from the airport to the spiraling position. The distance between the lidar site and the flight pattern is approx. 20 km.

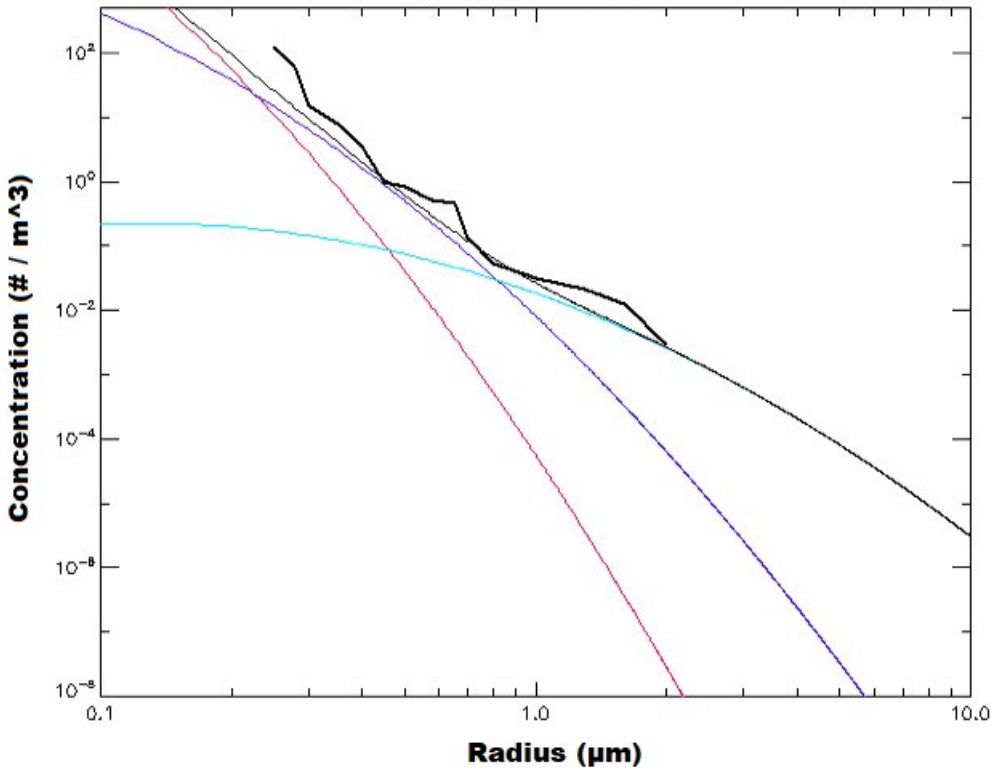

Figure 2: Size distribution computed from the OPC data (bold black line), together with the total theoretical distribution (thin black line) and theoretical distributions for the three different modes: fine mode (soot and pollution, red line), accumulation mode (water-soluble aerosols, violet line) and coarse mode (sea salt, light blue line).

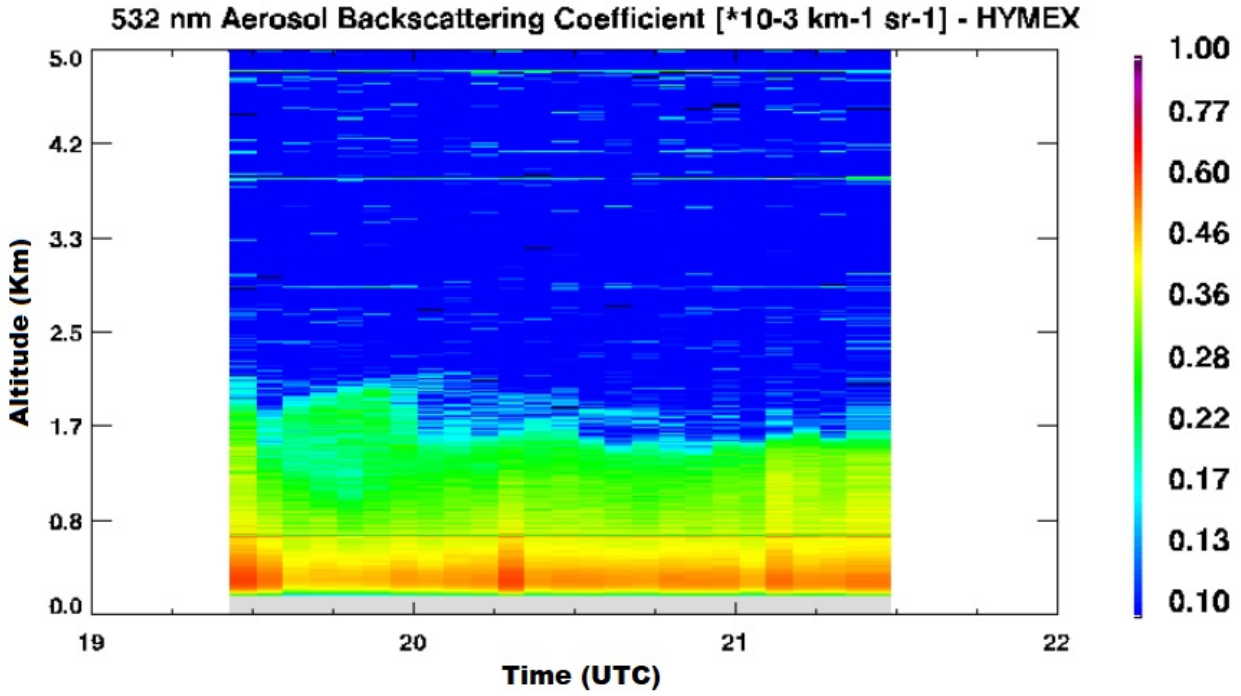

595

Figure 3: Time evolution of the particle backscattering coefficient at 532 nm over the time interval 19.30-21.30 UTC on 13 September 2012.

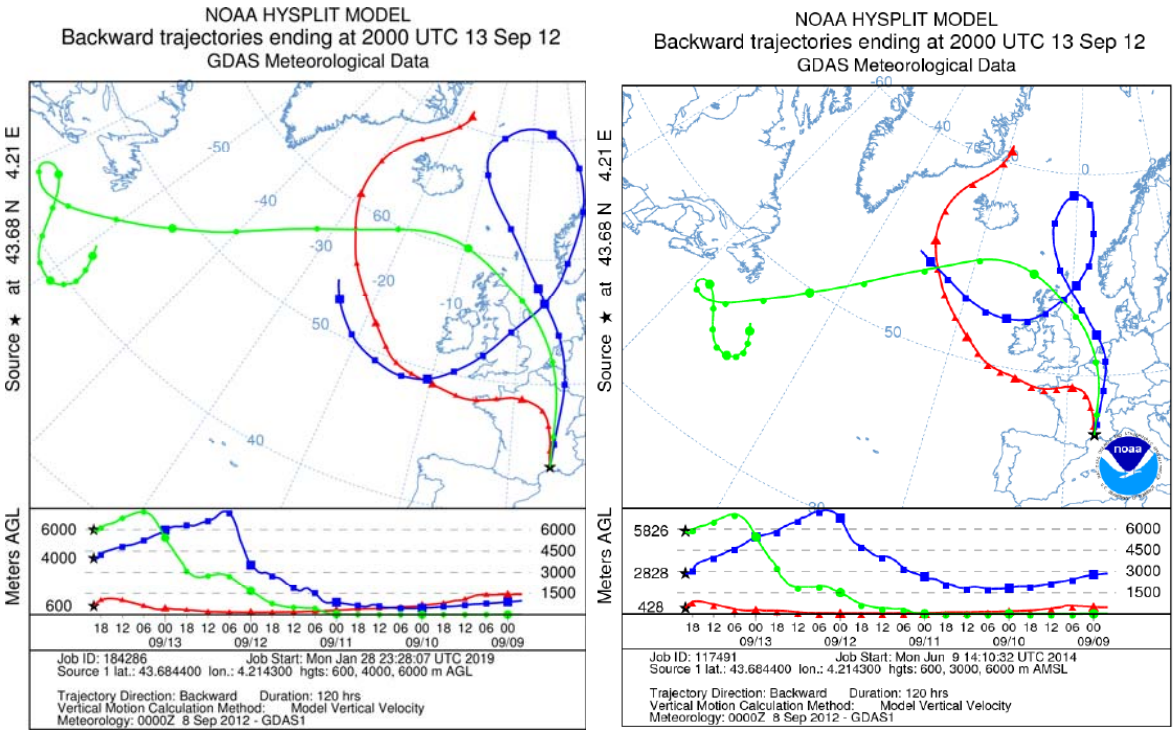

Figure 4: Air masses back-trajectories at 600 m (red), 4000 m (blue) and 6000 m (green) ending over the lidar site at 20 UTC on 13 September 2012.

	$\bar{r}$ (μm)	σ	m_r (355 nm)	m_i (355 nm)	m_r (532 nm)	m_i (532 nm)
Soot	0.012	2.00	1.75	4.65×10^{-1}	1.75	4.44×10^{-1}
Water soluble	0.024	2.24	1.53	5.00×10^{-3}	1.53	6.00×10^{-3}
Dust-like	0.471	2.51	1.53	8.00×10^{-3}	1.53	8.00×10^{-3}
Sea-salt (fine)	0.300	2.51	1.39	1.20×10^{-7}	1.38	3.70×10^{-9}
Sulphate	0.069	2.03	1.45	1.00×10^{-8}	1.43	1.00×10^{-8}
Sea-salt (acc.)	0.400	2.03	1.39	1.20×10^{-7}	1.38	3.7×10^{-9}
Mineral	0.270	2.67	1.53	1.70×10^{-2}	1.53	5.50×10^{-3}

Table 1: Modal radius, standard deviation and refractive index (real and imaginary part) for the different considered aerosol components (from d'Almeida *et al*., 1991).

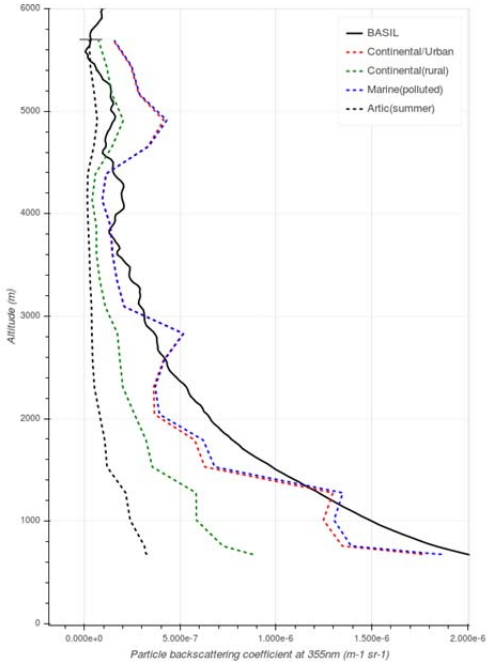

Figure 5: Vertical profiles of the measured (black line) and simulated particle backscattering coefficient at 355 nm over the time interval 19.55-20.35 UTC on 13 September 2012. The error bar in lidar measurements accounts for the statistical uncertainty.

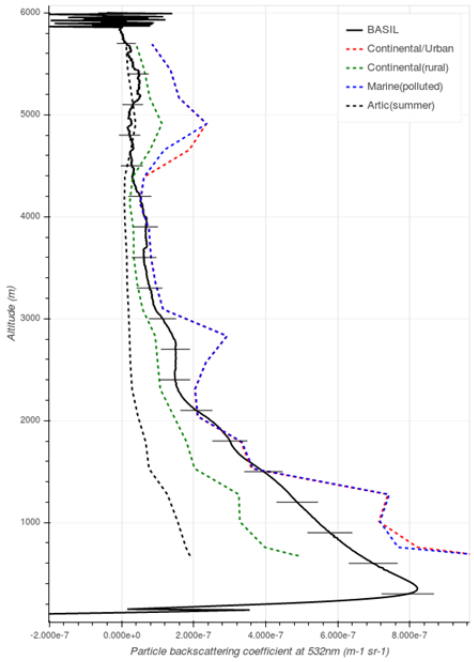

Figure 6: Same as Fig. 5 but for the particle backscattering coefficient at 532 nm.

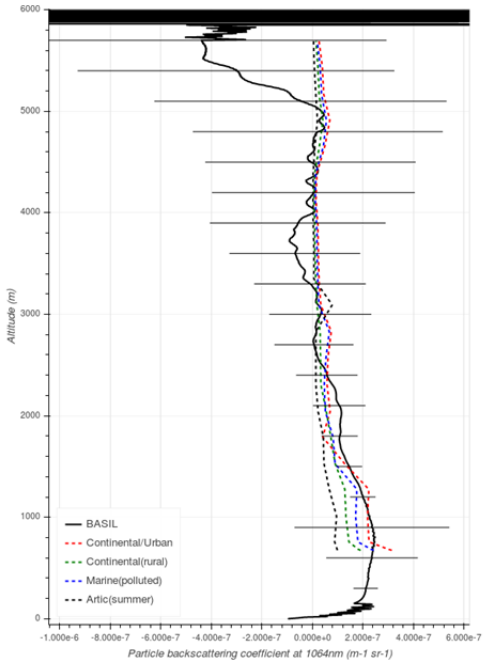

Figure 7: Same as Fig. 5 but for the particle backscattering coefficient at 1064 nm

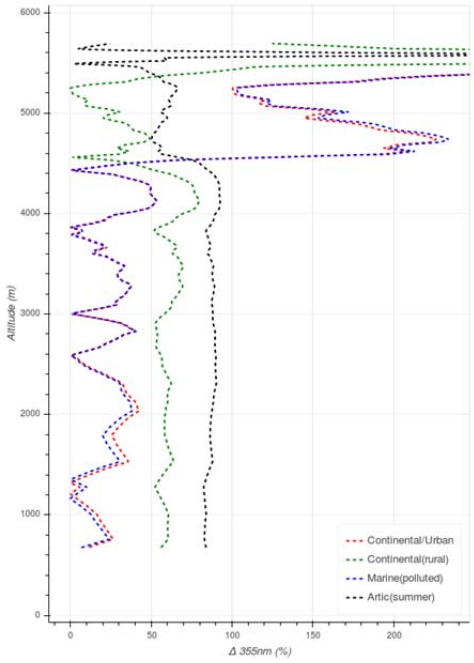

Figure 8: Deviation, expressed in percentage, between measured and simulated particle backscattering coefficient profiles at 355 nm. Simulated profiles are: Arctic Summer (black dashed line), Continental/Urban (red dashed line), Marine (polluted) (blue dashed line) and Continental (rural) (green dashed line).

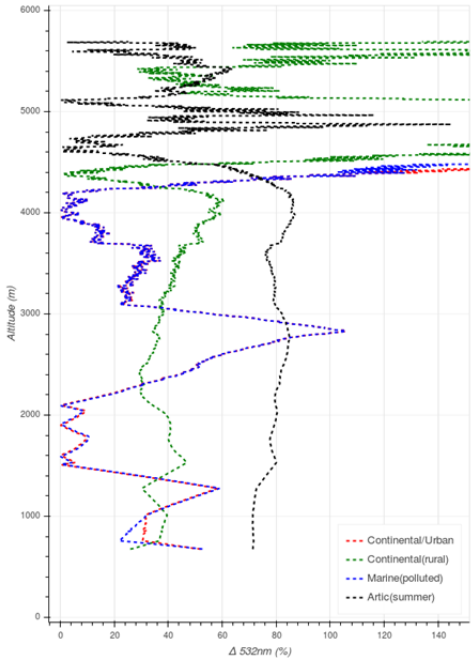

615

Figure 9: Same as figure 8, but obtained considering particle backscattering coefficient profiles at 532 nm.

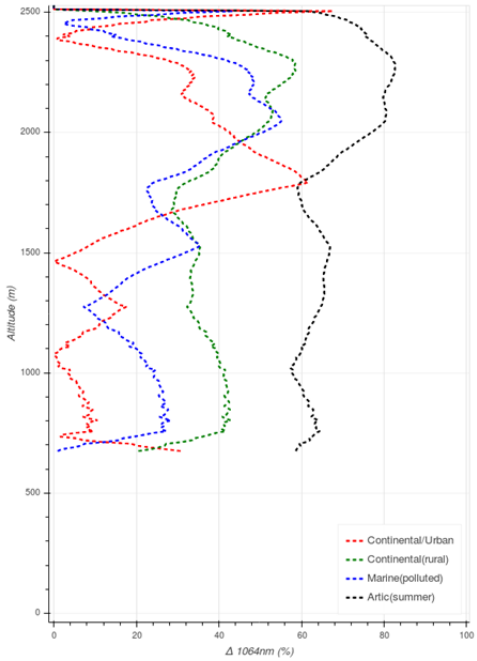

Figure 10: Same as figure 8, but obtained considering particle backscattering coefficient profiles at 1064 nm up to 2500 m.

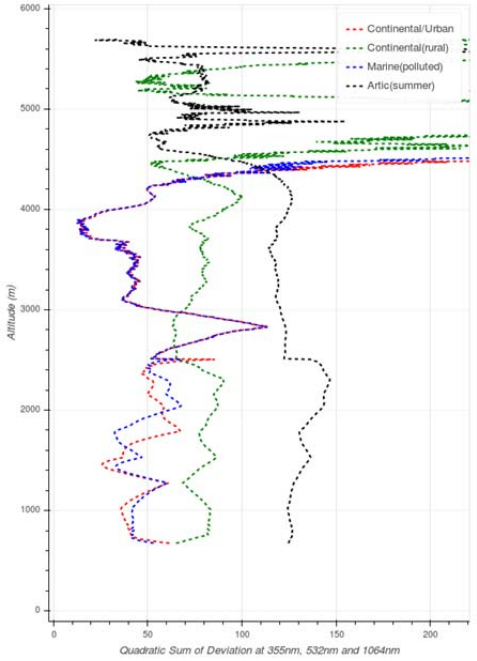

620

Figure 11: Total deviation, in percentage, between measured and simulated particle backscattering coefficient profiles at 355, 532 nm and 1064 nm (until 2500m) for the different aerosol components. Simulated profiles are: Arctic Summer (black dashed line), Continental/Urban (red dashed line), Marine (polluted) (blue dashed line) and Continental (rural) (green dashed line).

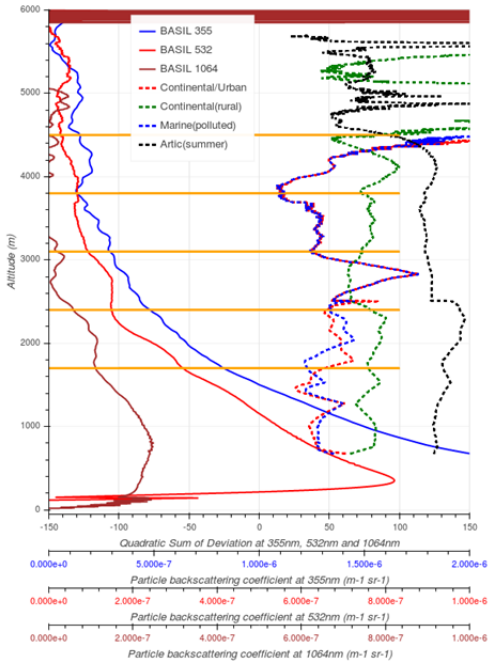

Figure 12: Total deviation, in percentage, between measured and simulated particle backscattering coefficient profiles for the different aerosol components (Arctic Summer: black dashed line, Continental/Urban: red dashed line, Marine polluted: blue dashed line; Continental rural: green dashed line) and measured particle backscattering profiles at both 355 (blue line) and 532 nm (red line). The horizontal blue and red axes refer to the particle backscattering coefficient at 355 and 532 nm, respectively, while the horizontal black axis refers to the total deviations. Horizontal orange lines are also drawn at specific altitudes to identify different aerosol types in support of the interpretation of the reported results.

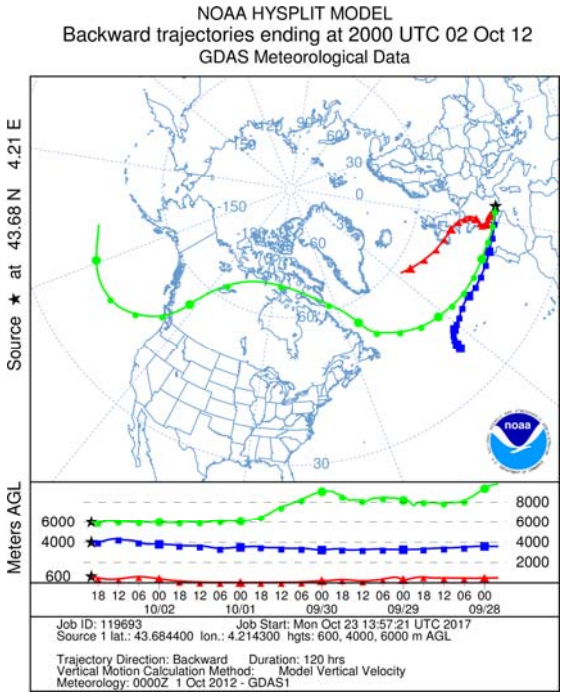

635 **Figure 13: Back-trajectories at 600 m (red), 4000 m (blue) and 6000 m (green) ending on the lidar site at 20 UTC on 02 October 2012.**

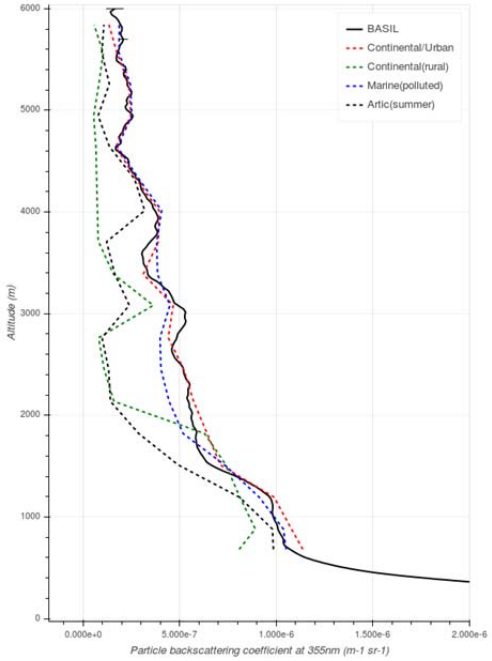

Figure 14: Vertical profiles of measured (black line) and simulated particle backscattering coefficient at 355 nm over the time interval 19.43-20.27 UTC on 02 October 2012. Simulated particle backscatter profiles include five distinct components:

Continental/Urban (red dashed line), Continental (rural) (green dashed line), Arctic Summer (black dashed line) and Marine (polluted) (blue dashed line). The error bar in lidar measurements accounts for the statistical uncertainty.

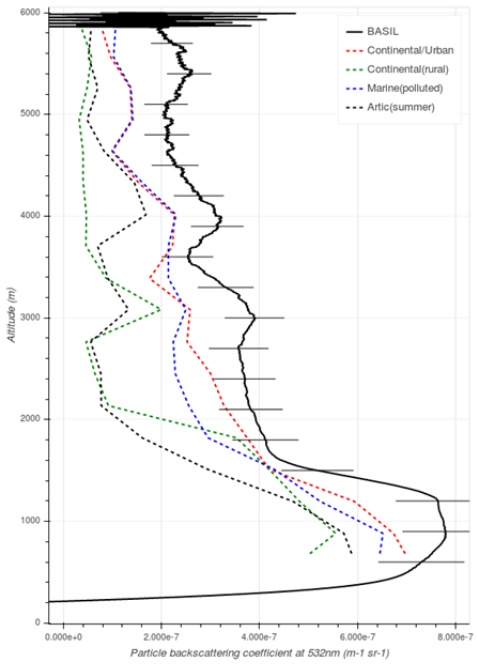

Figure 15: Same as figure 14, but with particle backscattering coefficient profiles at 532 nm.

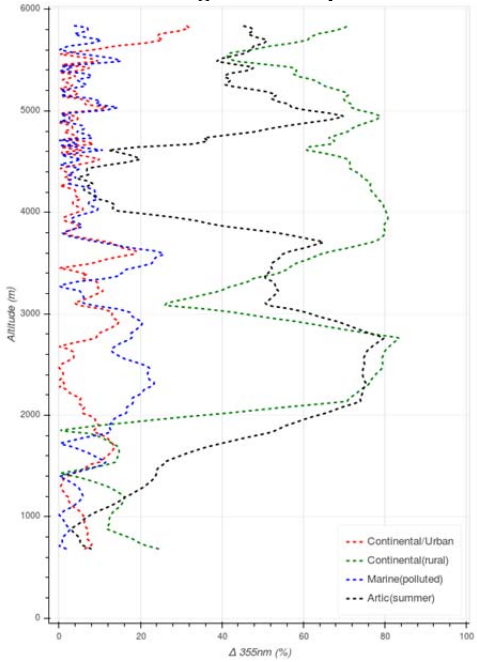

Figure 16: Deviation, expressed in percentage, between measured and simulated particle backscattering coefficient profiles at 355 nm. Simulated profiles are: Arctic Summer (black dashed line), Continental/Urban (red dashed line), Marine (polluted) (blue dashed line) and Continental (rural) (green dashed line).

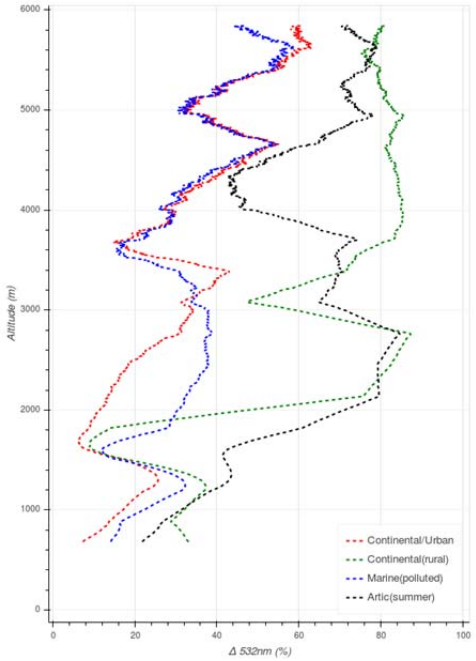

Figure 17: Same as figure 16, but obtained considering particle backscattering coefficient profiles at 532 nm.

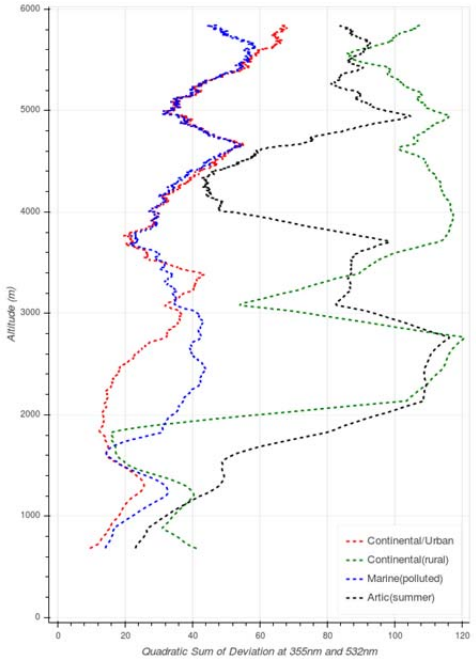

650

Figure 18: Total deviation, in percentage, between measured and simulated particle backscattering coefficient profiles at 355 and 532 nm for the different aerosol components. Simulated profiles are: Arctic Summer (black dashed line), Continental/Urban (red dashed line), Marine (polluted) (blue dashed line) and Continental (rural) (green dashed line).

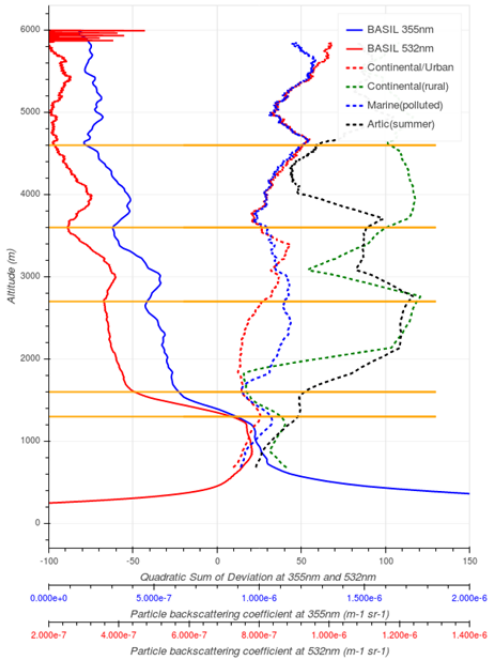

Figure 19: Total deviation, in percentage, between measured and simulated particle backscattering coefficient profiles for the different aerosol components (Arctic Summer: black dashed line, Continental/Urban: red dashed line, Marine polluted: blue dashed line; Continental rural: green dashed line) and measured particle backscattering profiles at both 355 (blue line) and 532 nm (red line). The horizontal blue and red axes refer to the particle backscattering coefficient at 355 and 532 nm, respectively, while the horizontal black axis refers to the total deviations. Horizontal orange lines are also drawn at specific altitudes to identify different aerosol types in support of the interpretation of the reported results.